UNIVERSITY of York

This is a repository copy of *Model of advanced recording system for application in heat-assisted magnetic recording*.

White Rose Research Online URL for this paper:
https://eprints.whiterose.ac.uk/223470/

Version: Published Version

Article:
Pantasri, Wasan, Meo, Andrea, Chureemart, Phanwadee et al. (4 more authors) (2025) Model of advanced recording system for application in heat-assisted magnetic recording. Scientific reports. 2776. ISSN 2045-2322

https://doi.org/10.1038/s41598-025-87044-1

Reuse
This article is distributed under the terms of the Creative Commons Attribution-NonCommercial-NoDerivs (CC BY-NC-ND) licence. This licence only allows you to download this work and share it with others as long as you credit the authors, but you can't change the article in any way or use it commercially. More information and the full terms of the licence here: https://creativecommons.org/licenses/

Takedown
If you consider content in White Rose Research Online to be in breach of UK law, please notify us by emailing eprints@whiterose.ac.uk including the URL of the record and the reason for the withdrawal request.

White Rose university consortium
Universities of Leeds, Sheffield & York

eprints@whiterose.ac.uk
https://eprints.whiterose.ac.uk/

scientific reports

Check for updates

OPEN

Model of advanced recording system for application in heat-assisted magnetic recording

Wasan Pantasri[1], Andrea Meo[1,2], Phanwadee Chureemart[1], Asanee Suntives[3], Kotchakorn Pituso[3], Roy W. Chantrell[1,4] & Jessada Chureemart[1]✉

Heat assisted magnetic recording (HAMR) technology is considered a solution to overcome the limitations of perpendicular magnetic recording and enable higher storage densities. To improve and understand the performance of magnetic writers in HAMR technology, it is crucial to possess a comprehensive understanding of both the magnetic field generated during the writing process and the thermal effects induced by the laser. In this work, we have developed a micromagnetic HAMR model with atomistic parameterization. To demonstrate the applicability of the developed model, it is employed to investigate the Write Current Assisted Percentage (WCAP) measurement which is characterized by the difference in laser current needed to erase a narrow data track with and without assistance of the magnetic field generated by the writer. This value allows us to subsequently consider the strength of the magnetic field from the writer, which is difficult to evaluate experimentally. We study the effect of crucial factors such as the laser current, the frequency of the writing field and the grain size distribution of the recording media on the WCAP. The results reveal that, under a high applied field, a correspondingly elevated WCAP is generated. This observation suggests that the track undergoes erasure to approximately half of its amplitude, achieved through the utilization of a low peak temperature. The comparison between simulation and experimental data demonstrates excellent agreement and acts as a validation of the underlying principle of WCAP. Additionally, we explore theoretically the impact of the writer frequency, and the results suggest that lower frequencies give rise to an increase in WCAP. This implies that lower frequencies allow for a reduction in temperature required to erase the track. The technique is valuable in evaluating and contrasting the magnetic behavior of various write pole configurations, examining the frequency responses of different designs, and comparing different media.

Heat assisted magnetic recording (HAMR)[1–4] technology holds significant promise as a solution to attain increased areal density and to transcend the limitations associated with the conventional perpendicular magnetic recording (PMR)[5,6] technology. To increase areal density, high anisotropy magnetic materials are required as storage media[7–9]. This serves to enhance the stability of small data bits. As the dimensions of these elements are decreased to satisfy the demands of high data density, the obligatory augmentation of media anisotropy poses a barrier to magnetic switching due to the limited fields which can be generated using inductive technology. HAMR enables the writing of small data bits using relatively low magnetic fields, which is achieved by utilizing heat to temporarily reduce the anisotropy of the recording medium. This process is accomplished through a unified head mechanism, employing heat application via a near-field transducer (NFT) stimulated by laser diode light[10–12], while the magnetic field is administered using a nearby magnetic recording head similar to traditional perpendicular magnetic recording setups as shown in Fig. 1. However, although this method reduces the required magnetic field strength from the recording head, the magnitude of the field and the rise time still remain crucial factors in establishing low-noise transitions effectively[13–16].

It is important to characterize the scale of the magnetic field strength and the thermal energy employed during the writing process. There are studies in the literature, both theoretical and experimental works[17–24], on the effects of temperature and magnetic properties of the recording medium on the performance of the writing process in hard disk drives (HDDs). However, a study focusing on writing performance for realistic systems is lacking, specifically aimed at the design of HAMR media and magnetic writers. In this study, we have

[1]Department of Physics, Mahasarakham University, Mahasarakham 44150, Thailand. [2]Department of Electrical and Information Engineering, Politecnico of Bari, 70125 Bari, Italy. [3]Seagate Technology, Teparuk, Samutprakarn 10270, Thailand. [4]School of Physics, Engineering and Technology, University of York, York YO10 5DD, UK. ✉email: jessada.c@msu.ac.th

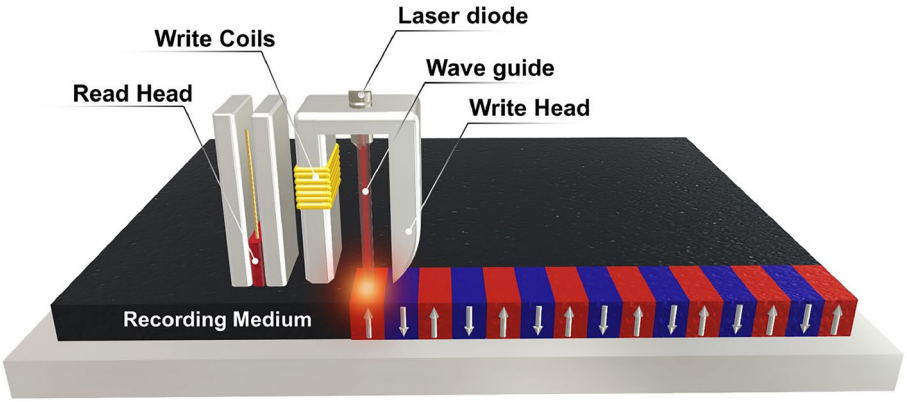

Fig. 1. A schematic of the essential elements utilized in the writing procedure of HAMR technology.

exploited a hierarchical approach that combines micromagnetic simulations and atomistic spin simulations [25–29] to obtain an accurate description of the magnetic properties of the system as well as the magnetization processes at elevated temperature, such as in HAMR.

The WCAP experiment is a fundamental test that Seagate and other recording manufacturers utilize to assess the writing performance of the device. This, along with other factors such as the evaluation of the signal to noise ratio (SNR) and estimation of the bit error rate (BER), represents a complete tool set for obtaining a comprehensive assessment of the device's performance. SNR and BER are standard experiments, well understood and developed for the characterization of media for perpendicular magnetic recording (PMR). However, the HAMR technology relies on the modification of materials properties through laser heating, introducing new physical factors into the media characterization beyond previous practices. WCAP is one such experiment which provides useful feedback for the magnetic writer design for HAMR heads. Both the current response and frequency response can be determined independently. If the anisotropy versus temperature profile of the recording medium is known, the magnetic field from the head can be estimated. However, the underlying physical processes involved in the determination of WCAP have not been investigated in detail. Here we present an analysis of the WCAP experiment using the micromagnetic model which is called MARS (Models of Advanced Recording Stystems). MARS [25] is an open source multi-timescale micromagnetic code designed for the modelling of advanced recording system which is described in detail in the methods section. The results give good agreement with experiment, supporting the determination of parameters using the WCAP method.

To validate the model's accuracy, we make a direct comparison of the WCAP between simulation and experimental data. This is a fundamental test utilized by industry to characterize the write performance of the device. In experimental settings, directly measuring the magnetic field emitted by the writing head proves to be quite challenging[30,31]. As an alternative, Saunders and Zhao [32] proposed a method to calculate the magnetic field from the writing head by utilizing the WCAP metric. WCAP represents the percentage by which the laser current is reduced as a result of the assistance provided by the magnetic field of the writer. Our objective is firstly to introduce a methodology that utilizes the MARS code to quantify the WCAP within a practical system. Subsequently, we describe a comparison between these findings and experimental observations. Finally, we explore how the frequency of the writer impacts WCAP in order to enhance the efficiency of the magnetic writer. We expect that this study will serve as a valuable reference for comparing the magnetic response to distinct write pole configurations, to assess the frequency response of various designs, and evaluating media within experimental contexts.

Results

In the following, we present the study of the impact that different parameters have on the WCAP. The study is performed utilizing a multiscale model, whose details of the and parameters are given in the "Methods", corroborated by experimental results. The relevant parameters utilized in these calculations are detailed in Table 1.

WCAP simulation

We first reproduce the experimental WCAP procedure described by Saunders and Zhao [32] and detailed in the "Methods". A reference track is created by writing a single-tone signal onto a 60 nm x 120 nm magnetic film at a temperature near the film's transition temperature (approximately 750 K) under an applied magnetic field of 1 T, as shown in Fig. 2a. The erasure of a single-tone magnetic track is shown in Fig. 2b, c, where two different laser currents are used to achieve temperatures of 650 K and 700 K, respectively, in the absence of a magnetic field. At 700 K we clearly observe degradation of the magnetic texture with about half of the grains within the track have undergone demagnetization. This allows us to extract the median Curie temperature of the film (T_c).

Next, we repeat the erasure with the addition of a magnetic field to extract the writing temperature (T_W) as the temperature at which the track's amplitude is reduced to half of its original value. By comparing panels (a–c), we can see how grains located at the system edges along the cross track direction are not affected during the erasure. This is because for these T_W, the temperature profile at the edges of the track is not enough to reverse

Parameters	Symbol	Value	Unit
Exchange constant	J_{ij}	6.81×10^{-21}	J/link
Magnetic anisotropy energy	k_{u}	2.63×10^{-22}	J/atom
Magnetic spin moment	μ_{s}	3.63	μ_{B}
Magnetic anisotropy energy density	K_{u}	9.37×10^{7}	erg/cc
Saturation magnetization	M_{s}	1067	emu/cc
Curie temperature	T_{c}	690	K
Gilbert damping	λ	0.10	
Full Width half Maximum	$\mathrm{FWHM}_{\mathrm{X,Y}}$	100,120	nm
NFT-to-pole spacing	*NPS*	34	nm
Skew angle	*SK*	0	degree
Read-head velocity	*v*	22	m/s
Bit length	*BL*	30	nm
Track width	*TW*	50	nm

Table 1. Simulation parameters for the investigated systems.

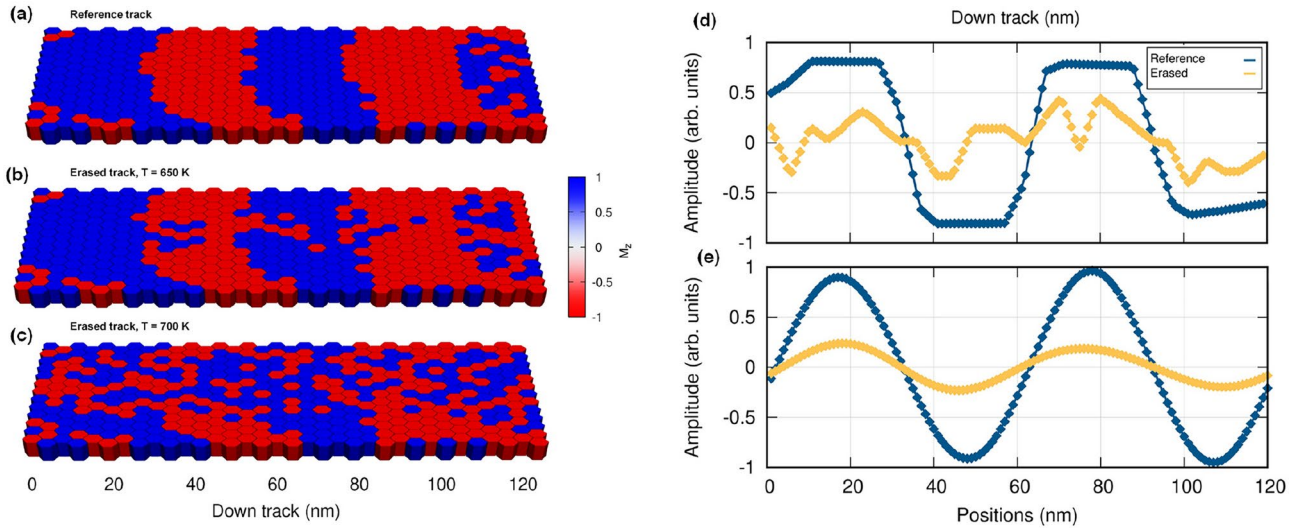

Fig. 2. The magnetization configuration after (**a**) The writing process under a magnetic applied field of 1.0 T and a temperature of 750 K. (**b**) The erased process at temperature of 650 K without a magnetic applied field and (**c**) The erased process at temperature of 700 K without a magnetic applied field for a film of dimensions 60 nm x 120 nm. The average track amplitude for the reference (blue) and the erased (yellow) track at a writing temperature of 700 K and magnetic field of 1 T as a function of position obtained (**d**) without and (**e**) with a low-pass filter.

the grains magnetization. Figure 2d shows the readback signal for the reference track and erased tracks under a magnetic field of 1 T and a temperature of 700 K, where Fig. 2e presents data smoothed by post processing the readback signal with a low-pass filter. An example is presented in Fig. 3, where the average erased track amplitude extracted for various magnetic field strengths is plotted as a function of temperature to obtain T_C and T_{W}, known T_A. Therefore, we calculate WCAP as:

$$WCAP = 100\% \times \left[1 - \frac{(T_W - T_A)}{(T_C - T_A)}\right]. \tag{1}$$

Effect of magnetic field strength

To investigate the effect of the magnetic field on WCAP, we initially explore how the WCAP calculations depend on magnetic field strength. The system operates using a single tone at 25% of the reference frequency. The reference frequency is 0.56 GHz, which corresponds to a bit length (BL) of around 30 nm and a track width (TW) of 50 nm. Figure 3 shows the average erased track amplitude as a function of temperature for various strengths of an applied magnetic field, ranging from 0 to 2.0 T. The results demonstrate that a strong applied magnetic field requires lower temperatures to reduce the average track amplitude to half its initial value. In the absence of an applied magnetic field, higher temperatures are needed to decrease the average track amplitude

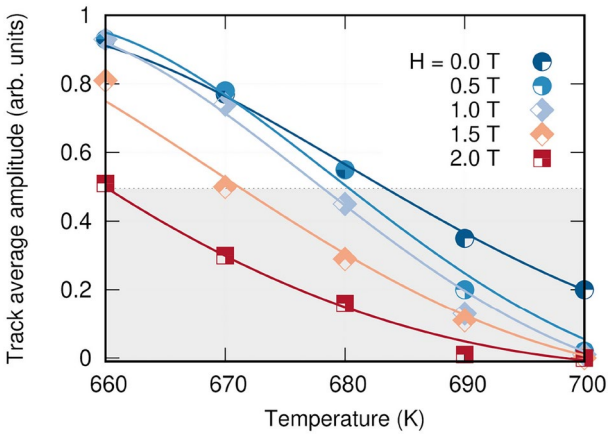

Fig. 3. The normalized average track amplitude as a function of temperature for various applied magnetic field strengths ranging from 0 to 2.0 T at 10% of reference frequency.

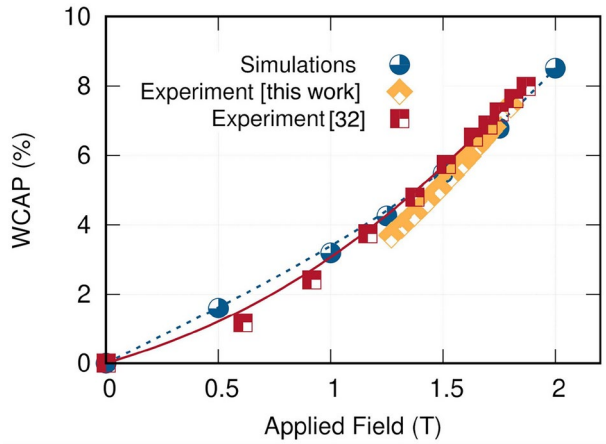

Fig. 4. The Write Current Assist Percentage plotted against the applied field, comparing simulation results obtained from MARS model with our experimental measurement and the measurement by Saunders et al.[32].

to half of its initial value. The temperature at which the average amplitude reaches 0.5 without assistance from a magnetic field has been identified as 686 K, denoted as T_c. With the application of a magnetic field of 2.0 T, the corresponding temperature is found to be 661 K, represented as T_W.

Figure 4 illustrates the relationship between the write current assist percentage (WCAP) and the applied field, comparing simulation (blue) and experimental results obtained in this work (yellow) with the reference experimental data from Ref.[32] (red). The system subjected to a strong applied magnetic field shows a proportionally higher WCAP, due to the assistance of a robust magnetic field in achieving a reduction of the track's average amplitude to half of its initial value at lower temperatures (T_W). Importantly, there is a congruence between the WCAP values obtained from simulation, Seagate experimental data and data by Saunders *et al.*[32]. The comparative results indicate that the model is precise and can serve as a useful tool to support and guide experiments.

Effect of erasing frequency

In this section, we explore the impact of writer frequency, a crucial factor affecting WCAP. The frequency of the writer controls the speed or duration of the writing process in HAMR. We compute the WCAP as a function of the applied magnetic field while altering the writer frequency within the range of 0.75 times the reference frequency to 0.95. Figure 5a illustrates the WCAP as a function of the applied field, considering various writer frequencies. The calculated results demonstrate a direct correlation between WCAP and temperature. Figure 5b illustrates the comparison of WCAP between magnetic applied fields of 1 T and 2 T. The results indicate that the WCAP at a magnetic applied field of 2 T is greater than that at 1 T. Moreover, when the writing head frequency reaches a higher value (0.95 times the reference frequency), the WCAP decreased. On the contrary, lowering the writing head frequency (0.75 times the reference frequency) resulted in an increase in WCAP, in agreement with the experimental findings of this work. At higher writing head frequencies, the system demanded elevated temperatures for demagnetization, owing to the reduced assistance from the writer.

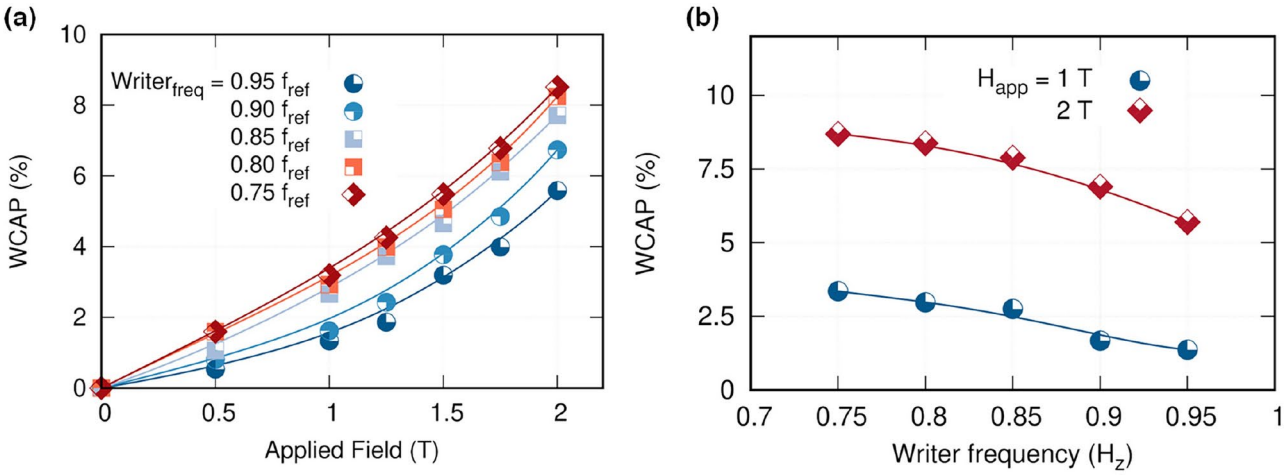

Fig. 5. (**a**) The WCAP as a function of a magnetic applied field, considering different writer frequencies ranging from 0.75 times the reference frequency to 0.95. and (**b**) The WCAP as a function of a writer frequencies, considering different magnetic applied field ranging from 1.0 T to 2.0 T.

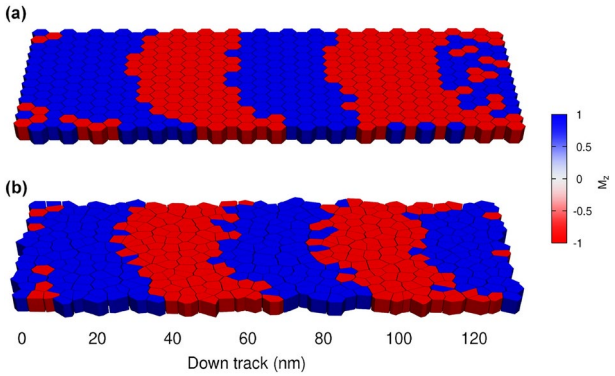

Fig. 6. Magnetization configuration after the writing process under an external magnetic field of 1.0 T at a temperature of 750 K, comparing (**a**) absence of grain size distribution and (**b**) presence of grain size distribution $\sigma_G = 0.2$. Colors represent the z–component of the magnetization (blue=$+z$, red=$-z$, white=in-plane).

A high WCAP allows for a reduction in laser current during track erasure or writing, attributed to the enhanced assistance provided by the writer. In HAMR systems, excessive laser currents during the writing process are unnecessary as they can degrade the NFT material and negatively impact the magnetic media's properties. Additionally, writing tracks at elevated temperatures can compromise laser stability, leading to issues such as mode hopping or power fluctuations.

The effect of grain size distribution

To understand the magnetic properties of recording media and their influence on writing performance, we study the effect of grain size distribution on WCAP. Figure 6 illustrates the magnetic configuration of the track after the final writing process, comparing the scenarios of no grain size distribution (a) with grain size distribution (b).

We can clearly observe a decrease in the sharpness of the transitions between bits (red and blue regions) in the case of grain size distribution. This affects negatively both the read back of the signal and the writing performance. Figure 7 presents the WCAP plotted as a function of the applied field, comparing the case of no distribution with a grain size distribution modeled as a Gaussian with standard deviation $\sigma_G = 0.2$. The results indicate that a high grain size distribution leads to a decrease in WCAP. This can be attributed to the fact that a higher grain size distribution results in a distribution of energy barriers and distribution of Curie temperature within the grains [33]. Consequently, higher temperatures are required to effectively reduce the average track amplitude. Maintaining a high level of writing process performance in HAMR involves controlling the grain size distribution, which plays a crucial role in influencing the writing performance. In summary, a high grain size distribution in HAMR can lead to variations in thermal stability, non-uniform thermal profiles, and inconsistent magnetic properties. All these factors collectively lead to a reduced Write Capability or WCAP, which, in turn, necessitates higher temperatures during the erasing process. In the experiment, varying the grain size distribution

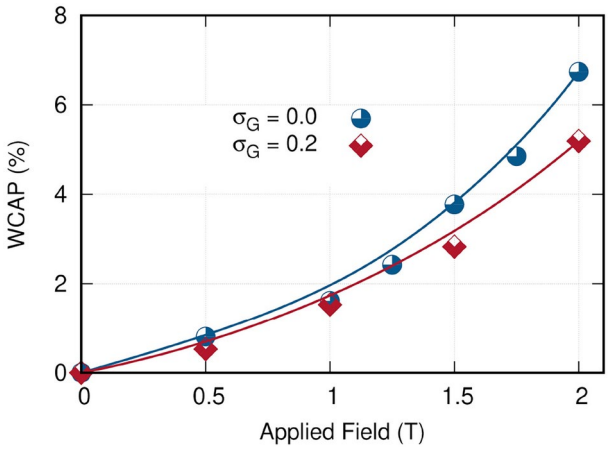

Fig. 7. The Write Current Assist Percentage as a function of the applied field with different grain size distribution and writer frequency of 0.9.

and material properties is very challenging. However, by using our model, we can systematically investigate how grain size distribution, material properties, and other factors impact the writability and reliability of HAMRs. This approach allows us to understand and optimize these parameters effectively.

Discussion and conclusions

We have developed a multiscale approach based on an atomistically parameterized micromagnetic formalism to model HAMR media that can, through the accurate description of the physical principles involved in the writing process, be utilized to reach a deeper understanding and improve HAMR technology. We have focused our analysis on the WCAP procedure, a set of measurements developed at Seagate aimed at assessing the write performance of the device, that is often employed during the development phase. We have successfully reproduced the WCAP test methodology with our model and we have employed it to study the effect of crucial factors to determine the performance of HAMRs such as the laser current, the frequency of the writing field and the grain size distribution of the magnetic film. We have compared our results with experimental WCAP measurements performed at Seagate obtaining an excellent agreement, thus validating our approach. Moreover, this consistency underlines the potential of our comprehensive approach as a valuable tool to facilitate the progression of future HAMR technology.

Methods

Experimental procedure

Since the magnetic field cannot be directly measured on a spinstand tester, Saunders and Zhao proposed an approach for the magnetic field measurement based on amplitude, called the write current assist percentage (WCAP) test[32]. In the measurement, a narrow track is written on the medium using a certain single-tone frequency and very low laser current. The average amplitude of the written microtrack is read using a narrow band filter of the write frequency. The test then performs overwrite on that microtrack to erase it with the writer coil on, with different frequency, and varying laser current. The residual amplitude of the microtrack is read after each overwrite. The laser current that reduces the residual amplitude to half of its original amplitude is defined as the writing laser current (I_{TW}). The experiment is then replicated using different laser currents only for the purpose of thermal erasure during overwriting, with the track being reset after each attempt at erasure. It is assumed that the media grains are demagnetized when the residual amplitude is reduced to half of its original. Thus, the laser current that erases the microtrack amplitude to 50% is defined as the median Curie temperature laser current (I_{Tc}). This condition is interpreted as indicating that half of the grains within the track have reached the median Curie temperature I_{Tc} and have become demagnetized. This method provides a practical and reproducible way to estimate I_{TW} under our experimental conditions. Finally, WCAP is calculated as follows:

$$WCAP = 100\% \times [1 - (I_{T_{\mathrm{W}}}/I_{T_{\mathrm{c}}})]\,. \tag{2}$$

In this experiment, the spindle rotation speed is set to 7200 revolutions per minute. 16 recording heads are tested on the middle media radius with 0 degree skew angle. Measurements are made on the the same medium so that all heads are tested for the same medium Curie temperature. Each recording head uses the same write current that produces the highest average areal density of these heads. The heater power is also optimized to set the active fly clearance to 1.5 nm. Since the microtrack requires low laser current to make it narrow, the track amplitude is lower than the track that is written by normal operating laser current. Thus, the recording frequency for the probe microtrack is set to 50% of product linear density to obtain a decent track amplitude. The track amplitude is measured by the reader and then processed by a 4 GHz digitizer with narrow band digital filter with the same frequency of the written track. To avoid harmonic reading after the erasures, the overwriting frequency is set

to 95% of product linear density. After all test conditions are settled, the WCAP is then measured using the algorithm given in the following section. The experimental WCAP result of 16 recording heads and its applied field transfer function is shown in Fig. 4 as yellow squares. For comparison between the data of simulation and the experimental results of Ref.[32] are also shown in Fig. 4.

Theory

Multiscale model of the writing process

To model and describe the magnetization dynamics of the writing process in HAMR, we employ the Model of Advanced Recording Systems (MARS) package [25,34], an open source multi-timescale micromagnetic code designed for the modelling of advanced recording systems. The software allows for the selection of different numerical solvers to address different phenomena and time scales. Since HAMR technology relies on heating the magnetic film up to temperature close to the Curie temperature (T_c) to assist the writing process, we describe the system dynamics by solving the Landau-Lifshitz-Bloch (LLB) equation [35]. In the LLB formalism the magnetization length is not constant, differently from the Landau-Lifshitz-Gilbert (LLG) model. This allows to account for the reduction of magnetic order as the temperature increases, an aspect import at temperatures close to T_c.

The LLB equation is derived in a classical model where spin-bath interactions are described by stochastic Langevin fields and spin-spin interactions are treated within the mean-field approximation. Then the LLB equation can be derived exactly from the Fokker-Planck equation, if the external conditions change slowly enough. In a numerical investigation, Chubykalo et al.[36] have compared the LLB model with an atomistic model of a grain, where the the exchange coupled atomic spin system, coupled to a Langevin thermostat plays the role of a heat bath for the macrospin. The dynamical properties, specifically the longitudinal and transverse relaxation times, are in full agreement between the atomistic and LLB approaches. In the case of HAMR the most rapidly varying external condition is the temperature increase induced by the laser. The temperature increase takes place over 10-100 ps which is much faster than the magnetization relaxation time which is on the sub-picosecond timescale both experimentally [37] and theoretically [38]. Consequently the LLB equation of motion is certainly valid for simulations of the HAMR process. The model requires as input the temperature dependence of the magnetic parameters, such as the saturation magnetization and magnetic anisotropy. To derive these input parameters we perform atomistic spin simulations by means of the open source VAMPIRE software package [39,40], thus adopting a hierarchical approach in which atomistic spin simulations yield the input parameters for the LLB model.

Atomistic spin model

The atomistic spin model relies on the assumption that the magnetic moment or spin can be localised on each atom. In VAMPIRE, the dynamics of each individual spin within the system is obtained by integrating the LLG equation of motion [16,40]:

$$\frac{\partial \vec{S}_i}{\partial t} = -\frac{\mu_0 \gamma}{1+\lambda^2}[\vec{S}_i \times \vec{\mathrm{H}}^i_{\mathrm{eff}} + \lambda \vec{S}_i \times (\vec{S}_i \times \vec{\mathrm{H}}^i_{\mathrm{eff}})], \tag{3}$$

where $\gamma = 1.761e11 T^{-1} s^{-1}$ is the electron gyromagnetic ratio, μ_0 is the permeability constant, λ is the Gilbert damping and represents the coupling of the spins to a thermal bath through which energy can be transferred into and out of the spin system. $\vec{\mathrm{H}}^i_{\mathrm{eff}}$ is the effective field acting on each spin obtained by differentiating the Hamiltonian ($\mathcal{H}$) with respect to the atomic spin moment (μ^i_s) and accounts for the interactions within the system. The effect of temperature is described as a white noise contribution that depends on damping, temperature and magnetic moment. This is done by adding to $\vec{\mathrm{H}}^i_{\mathrm{eff}}$ a Gaussian distribution in 3 dimensions whose first and second statistical moments of the distribution are given by:

$$\langle \xi_{i\alpha}(t) \rangle = 0, \tag{4}$$

$$\langle \xi_{ia}(t) \xi_{jb}(t\prime) \rangle = \frac{2\lambda k_B T}{\mu^i_s \gamma} \delta_{ij} \delta_{ab} \delta(t - t'), \tag{5}$$

where i, j label spins on the respective sites, $a, b = x, y, z$ are the vector component of $\bar{\xi}$ in Cartesian coordinates, t, t' are the time at which the Gaussian fluctuations are evaluated, T is the temperature, δ_{ij} and δ_{ab} are Kronecker delta and $\delta(t - t')$ is the delta function.

$\mathcal{H}$ describes the internal energy of the system and includes the following terms:

$$\mathcal{H} = -\sum_{i<j} J_{ij} \vec{S}_i \cdot \vec{S}_j - \sum_i k^i_u (\vec{S}_i \cdot \hat{e})^2 - \mu_0 \sum_i \mu^i_s \vec{S}_i \cdot \vec{\mathrm{H}}_{\mathrm{app}}. \tag{6}$$

The first term on the right hand side (RHS) is the isotropic exchange coupling between two neighboring spins represented by the exchange coupling constant J_{ij}, the second is the uniaxial magnetocrystalline anisotropy energy characterized by the on-site uniaxial energy constant k^i_u along the easy-axis $\hat{e}$, and the last term is the interaction with an external magnetic field $\vec{\mathrm{H}}_{\mathrm{app}}$. The intergranular exchange has been shown to decrease rapidly

with temperature [33,41] and is likely negligible at the elevated temperature of the HAMR write process, as is the magnetostatic interaction: consequently both contributions are neglected for computational efficiency.

Granular model

In our approach, the magnetic film is described as a granular film in which each grain is considered as an individual macrospin. Standard LLG formalism require that the length of the magnetization remain constant. However, while this can be considered true in atomistic approaches and in micromagnetics at zero or low temperature, it is not the case for temperature approaching T_c. To deal with finite temperature, Garanin[42] derived an LLB equation for a macrospin that accounts for the longitudinal relaxation of the magnetization, and thus its reduction with respect to its zero temperature value. Since this is crucial at high temperature such as those of HAMRs, this formalism is the most suited to be utilized in this work. In our model each grain is characterized by its magnetization vector $\vec{\mathrm{M}}$ whose magnetization dynamics is determined through the integration of the stochastic LLB equation [35]:

$$\frac{\partial \vec{\mathrm{m}}_i}{\partial t} = -\gamma_e \left(\vec{\mathrm{m}}_i \times \vec{\mathrm{H}}^i_{\mathrm{eff}}\right) - \frac{\gamma_e \alpha_{\parallel}}{{m_i}^2}\left(\vec{\mathrm{m}}_i \cdot \vec{\mathrm{H}}^i_{\mathrm{eff}}\right)\vec{\mathrm{m}}_i + \vec{\eta}_{\parallel} + \frac{\gamma_e \alpha_{\perp}}{{m_i}^2}\left[\vec{\mathrm{m}}_i \times \left(\vec{\mathrm{m}}_i \times \left(\vec{\mathrm{H}}^i_{\mathrm{eff}} + \vec{\eta}_{\perp}\right)\right)\right] \tag{7}$$

Here $\vec{\mathrm{m}}_i$ represents the normalized magnetization $\vec{\mathrm{M}}/M_{\mathrm{s}}$, m_i is the magnetization length of the i^{th} grain at finite temperature (T), $\vec{\eta}_{\perp}$ and $\vec{\eta}_{\parallel}$ are the thermal fields which describe the finite temperature effects on the perpendicular and parallel components of the magnetization, respectively. These are given by [43]

$$\begin{aligned} \langle \eta_i^{\mu} \rangle &= 0, \\ \langle \eta_i^{\perp}(0)\eta_j^{\perp}(t)\rangle &= \frac{2k_B T(\alpha_{\perp} - \alpha_{||})}{\gamma_e M_s V \alpha_{\perp}^2}\delta_{ij}\delta(t), \\ \langle \eta_i^{||}(0)\eta_j^{||}(t)\rangle &= \frac{2\gamma_e k_B T \alpha_{||}}{M_s V}\delta_{ij}\delta(t), \\ \langle \eta_i^{||}\eta_j^{\perp}\rangle &= 0 \end{aligned} \tag{8}$$

where $\mu = ||, \perp$ and indices i, j denote components x, y, z. $\alpha_{\parallel}$ and $\alpha_{\perp}$ are the longitudinal and transverse damping constants and depend on the phenomenological Gilbert damping parameter λ, γ_e is the electron gyromagnetic ratio, $\vec{\mathrm{H}}^i_{\mathrm{eff}}$ is the effective field:

$$\vec{\mathrm{H}}^i_{\mathrm{eff}} = \vec{\mathrm{H}}_{\mathrm{app}} + \vec{\mathrm{H}}_{\mathrm{ani}} + \vec{\mathrm{H}}_{\mathrm{intragrain}}, \tag{9}$$

where $\vec{\mathrm{H}}_{\mathrm{ani}}$ is the anisotropy field and $\vec{\mathrm{H}}_{\mathrm{intragrain}}$ is the intragrain longitudinal exchange field, which explains the reduction in magnetization length that occurs at finite temperatures. $\vec{\mathrm{H}}_{\mathrm{ani}}$ is described following Garanin's approach[42] as:

$$\vec{\mathrm{H}}_{\mathrm{ani}} = \left(m_x \hat{e}_x + m_y \hat{e}_y\right)/\tilde{\chi}_{\perp}, \tag{10}$$

where $\hat{e}_{x,y}$ is the unit vector perpendicular to the easy axis $\hat{e} = \hat{e}_z$ and $m_{x,y}$ are the reduced magnetization components along x, y–axes. $\tilde{\chi}_{\perp}$ is the reduced perpendicular susceptibility, which is a measure of the strength of the fluctuations of the components of the magnetization transverse to the easy-axis, and introduces the temperature dependence in $\vec{\mathrm{H}}_{\mathrm{ani}}$. It is worth noting that this expression reduces to the classical $2K_{\mathrm{u}}/M_{\mathrm{s}}$ at zero temperature.

The longitudinal field $\vec{\mathrm{H}}_{\mathrm{intragrain}}$ accounts for the exchange coupling between the atoms within the grain i, which is responsible for the reduction in the macroscopic magnetization length at finite temperature at the atomistic level. $\vec{\mathrm{H}}_{\mathrm{intragrain}}$ is written as:

$$\vec{\mathrm{H}}_{\mathrm{intragrain}} = \begin{cases} \dfrac{1}{2\tilde{\chi}_{\parallel}}\left(1 - \dfrac{m^2}{m_e^2}\right)\vec{\mathrm{m}}, & \text{if } T \leq T_c \\ -\dfrac{1}{\tilde{\chi}_{\parallel}}\left(1 + \dfrac{3}{5}\dfrac{T_{\mathrm{c}}}{T - T_c}m^2\right)\vec{\mathrm{m}}, & \text{otherwise} \end{cases} \tag{11}$$

where m is length of the grain reduced magnetization $\vec{\mathrm{m}}$, $m_e(T)$ is the equilibrium magnetization and $\tilde{\chi}_{\parallel}$ is the reduced parallel component of the susceptibility. $\tilde{\chi}_{\parallel}$ measures the fluctuations along the easy-axis and depends on temperature, as $\tilde{\chi}_{\perp}$. We wish to highlight that we have not included the magnetostatic contribution in our study since we are interested in the high temperature dynamics of magnetization. In fact, since in HAMR processes the temperature approaches T_{c} and the magnetization length shrink, so does the magnetostatic contribution that is proportional to the magnetization.

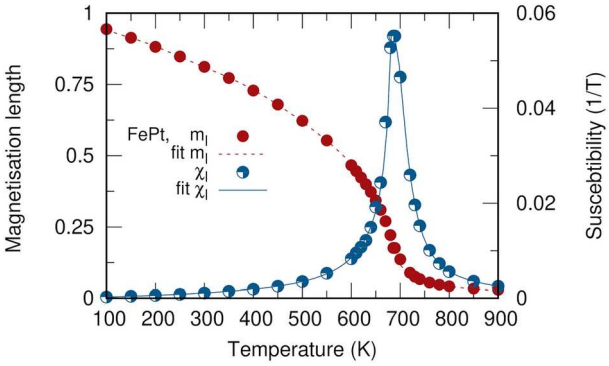

Fig. 8. The temperature dependence of normalized magnetization, $\mid M(T) \mid / M_s$ $(T = 0)$ and reduced longitudinal susceptibility obtained from atomistic model. Lines are fit of the data using the expressions given in Ref.[26].

HAMR dynamics

In HAMR technology, a crucial element is the near-field transducer (NFT), which generates localized heating up to and beyond the Curie temperature (T_c) to effectively lower the anisotropy field of the grains and facilitate the magnetization switching process. Within our approach, we model the HAMR process as a continuous laser recording procedure. The laser remains active throughout the entire writing duration, while the external magnetic field $H_{\rm app}$ changes direction from its previous orientation when a transition is to be recorded. The temperature distribution of the heat generated by the laser and focused by the NFT on the medium exhibits a Gaussian profile in down-track (x) and cross-track (y) directions:

$$T(x,y,t) = T_{\rm min} + (T_{\rm max} - T_{\rm min}) \exp\left[-\frac{1}{2}\left(\frac{x-vt}{\sigma_x}\right)^2\right] \cdot \exp\left[--\frac{1}{2}\left(\frac{y-C_y}{\sigma_y}\right)^2\right] \tag{12}$$

where, $T_{\rm min}$ is the initial temperature when the laser is off, usually room temperature, and $T_{\rm max}$ is the maximum temperature or writing temperature. σ represents the standard deviation of a Gaussian profile, where the full width at half maximum (FWHM) in the x and y directions is related to $\sigma_{x,y}$ as $\sigma_{x,y} = FWHM_{x,y}/\sqrt{8\ln 2}$, and C_y indicates the center of the write head in the cross-track direction.

Mutliscale parameterization

To reproduce and match experimental results, we generate in MARS a 60 nm x 120 nm film via Voronoi tessellation with grains of average diameter 5 nm and thickness 10 nm. To determine the input parameters required by MARS, we perform atomistic spin simulations of an individual hexagonal grain of the magnetic film [25–27,34]. Since the magnetic properties of the medium utilized in the experiments are proprietary, a generic FePt granular film is assumed. We consider chemically ordered tetragonally distorted fcc (fct) $L1_0$ FePt. $L1_0$ and map it to a distorted sc crystal structure [26,34,44,45] where the Pt moments, that are induced by proximity effect by Fe, are replaced by an effective enhanced Fe moment [46–48]. Table 1 provides a comprehensive summary of the material parameters utilized in this work, where we point out that $K_{\rm u}$ does not enter the formalism explicitly since $H_{\rm ani}$ is described via the perpendicular susceptibility.

To determine the temperature dependent equilibrium magnetization and susceptibility components of an individual grain we perform time evolution of the magnetization at different temperatures, as done in previous works [25–27]. We repeat each calculation 100 times with a different integration seed and take the average of the magnetization. To ensure good convergence of the results, we integrate the spin system for 100000 steps with an integration step $dt = 1fs$. Of these, the initial 50000 steps are only required to ensure that the spin system reaches thermal equilibrium and are therefore discarded, and only the last 50000 to 100000 steps contribute to the presented results. Figure 8 shows the temperature dependence of the reduced magnetization length m_l and the reduced longitudinal susceptibility $\tilde{\chi}_{\parallel}$ of an FePt grain, from which T_c can be also extracted. To obtain the input parameters for the LLB model we fit the atomistic data for the equilibrium properties following the same procedure described in Ref.[26].

WCAP modeling

To model the WCAP experimental procedure, we follow these steps:

1. A single tone track is written at a temperature close to the expected transition temperature of the magnetic film (750 K) in the presence of a magnetic field of 1 T. This represents the reference track. To simulate the read back process, the system is divided into 2D cells measuring 1 nm x 1 nm each. The read head is modeled as a boxcar of dimensions 1 nm x TW. The reading head is positioned at the track's center and then moved

along the track incrementally, one cell at a time. At each step, the system determines the magnetization by calculating the average magnetization within the reading head's area. We emphasize that this approach to read back considers an idealized reading head, implying that we assume the reader can discern the magnetization pattern without any loss of information.
2. Different laser currents (temperatures) are utilized to erase the microtrack in the absence of a coil current (zero magnetic field). When the temperature has reduced the microtrack's amplitude to half of its original value, we can assume that around half of the grains within the track have undergone demagnetization due to reaching the median Curie temperature (T_c). In this process, each track is read back, and the erased amplitude is acquired.
3. Next, the erase process is repeated with the application of a magnetic field. We define the temperature for which the microtrack amplitude is reduced to half of its original value as the writing temperature (T_W).
4. We post-process each individual signal through the application of a low-pass filter, aimed to attenuate the noise by eliminating the highest frequency component within the frequency spectrum. The cutoff frequency for this filter is determined based on the frequency of the shortest bit pattern that has been written, as detailed in Ref.[49].
5. Finally, the WCAP can be calculated, analogously to Eq. 2, as:

$$WCAP = 100\% \times \left[1 - \frac{(T_W - T_A)}{(T_C - T_A)}\right], \tag{13}$$

where T_W, T_c and T_A are the writing temperature, Curie temperature, and ambient temperature respectively. This calculation assumes that the temperature rise varies linearly with laser current. This assumption is reasonable for practical recording conditions in HAMR. The combination of heat and magnetic field results in a more linear erasure process compared to perpendicular magnetic recording (PMR), where the nonlinearity of the media's hysteresis loop dominates. In thermal erasure, the anisotropy of the media adjusts to match the magnetic field from the head, rather than the field adjusting to the media's anisotropy. This interplay supports the assumption of linearity in the relationship between temperature and laser current.

Data availability

The datasets used and/or analysed during the current study available from the corresponding author on reasonable request.

Received: 19 November 2024; Accepted: 15 January 2025
Published online: 22 January 2025

References

1. Rottmayer, R. E. et al. Heat-assisted magnetic recording. *IEEE Trans. Magn.* **42**, 2417–2421. https://doi.org/10.1109/TMAG.2006.879572 (2006).
2. Matsumoto, T. et al. Thermally assisted magnetic recording on a bit-patterned medium by using a near-field optical head with a beaked metallic plate. *Appl. Phys. Lett.* **93**, 031108. https://doi.org/10.1063/1.2960344 (2008).
3. Challener, W. et al. Heat-assisted magnetic recording by a near-field transducer with efficient optical energy transfer. *Nat. Photonics* **3**, 220–224. https://doi.org/10.1038/nphoton.2009.26 (2009).
4. Weller, D. et al. A HAMR media technology roadmap to an areal density of 4 tb/in^2. *IEEE Trans. Magn.* **50**, 1–8. https://doi.org/10.1109/TMAG.2013.2281027 (2014).
5. Weller, D. et al. Review Article: FePt heat assisted magnetic recording media. *J. Vac. Sci. Technol. B* **34**, 060801. https://doi.org/10.1116/1.4965980 (2016).
6. Evans, R. F. L., Chantrell, R. W., Nowak, U., Lyberatos, A. & Richter, H.-J. Thermally induced error: Density limit for magnetic data storage. *Appl. Phys. Lett.* **100**, 102402. https://doi.org/10.1063/1.3691196 (2012).
7. Rea, C. et al. Areal-density limits for heat-assisted magnetic recording and perpendicular magnetic recording. *IEEE Trans. Magn.* **52**, 1–4. https://doi.org/10.1109/TMAG.2016.2527735 (2016).
8. Chureemart, J., Chureemart, P., Pressesky, J., Nolan, T. & O'Grady, K. Media design and orientation in perpendicular media. *IEEE Trans. Magn.* **49**, 3592–3595. https://doi.org/10.1109/TMAG.2013.2245109 (2013).
9. Chureemart, P. et al. Hybrid design for advanced magnetic recording media: Combining exchange-coupled composite media with coupled granular continuous media. *Phys. Rev. Appl.* **8**, 024016. https://doi.org/10.1103/PhysRevApplied.8.024016 (2017).
10. Hu, Y., Wu, H., Meng, Y., Wang, Y. & Bogy, D. Head flying characteristics in heat assisted magnetic recording considering various nanoscale heat transfer models. *J. Appl. Phys.* **123**, 34303. https://doi.org/10.1063/1.5016873 (2018).
11. Shi, L. et al. Evaluating broader impacts of nanoscale thermal transport research. *Nanoscale Microscale Thermophys. Eng.* **19**, 127–165. https://doi.org/10.1080/15567265.2015.1031857 (2015).
12. Wu, A. et al. HAMR areal density demonstration of 1+ tbpsi on spinstand. *IEEE Trans. Magn.* **49**, 779–782. https://doi.org/10.1109/TMAG.2012.2219513 (2013).
13. Hohlfeld, J., Czoschke, P., Asselin, P. & Benakli, M. Improving our understanding of measured jitter (in HAMR). *IEEE Trans. Magn.* **55**, 1–11. https://doi.org/10.1109/tmag.2018.2872758 (2019).
14. Hernández, S. et al. Using ensemble waveform analysis to compare heat assisted magnetic recording characteristics of modeled and measured signals. *IEEE Trans. Magn.* **53**, 1–6. https://doi.org/10.1109/TMAG.2016.2612230 (2017).
15. Natekar, N., Tipcharoen, W. & Victora, R. Composite media with reduced write temperature for heat assisted magnetic recording. *J. Magn. Magn. Mater.* **486**, 165253. https://doi.org/10.1016/j.jmmm.2019.165253 (2019).
16. Victora, R. H. & Huang, P.-W. Simulation of heat-assisted magnetic recording using renormalized media cells. *IEEE Trans. Magn.* **49**, 751–757. https://doi.org/10.1109/TMAG.2012.2219300 (2013).
17. Vogler, C., Abert, C., Bruckner, F. & Suess, D. Landau-Lifshitz-Bloch equation for exchange-coupled grains. *Phys. Rev. B* **90**, 214431. https://doi.org/10.1103/PhysRevB.90.214431 (2014).
18. Suess, D. et al. Fundamental limits in heat-assisted magnetic recording and methods to overcome it with exchange spring structures. *J. Appl. Phys.* **117**, 163913. https://doi.org/10.1063/1.4918609 (2015).

19. Kanai, Y., Greaves, S. J., Yoshida, K. & Muraoka, H. Micromagnetic model analysis of high frequency heat-assisted magnetic recording. *J. Appl. Phys.* **117**, 17C506. https://doi.org/10.1063/1.4908024 (2015).
20. Torabi, A. F., Ek, J. V., Champion, E. & Wang, J. Micromagnetic modeling study of thermal gradient effect in heat-assisted magnetic recording (HAMR). *IEEE Trans. Magn.* **45**, 3848–3850. https://doi.org/10.1109/TMAG.2009.2023877 (2009).
21. Kalarickal, S., Tsoukatos, A., Hernandez, S., Hardie, C. & Gage, E. Adjacent track interference in heat-assisted magnetic recording: Impact and implications. *IEEE Trans. Magn.* **55**, 1–4. https://doi.org/10.1109/TMAG.2019.2897949 (2019).
22. Natekar, N. A. & Victora, R. H. Analysis of adjacent track erasure in the HAMR media. *IEEE Trans. Magn.* **57**, 1–11. https://doi.org/10.1109/TMAG.2020.3038805 (2021).
23. Zhu, J.-G.J. & Li, H. Correcting transition curvature in heat-assisted magnetic recording. *IEEE Trans. Magn.* **53**, 1–7. https://doi.org/10.1109/TMAG.2016.2614836 (2017).
24. Natekar, N. A., Roddick, E. & Brockie, R. M. Interplay of the thermal and magnetic fields in HAMR. *IEEE Trans. Magn.* **58**, 1–8. https://doi.org/10.1109/TMAG.2021.3122981 (2022).
25. Rannala, S. E. et al. Models of advance recording systems: A multi-timescale micromagnetic code for granular thin film magnetic recording systems. *Comput. Phys. Commun.* **279**, 108462. https://doi.org/10.1016/j.cpc.2022.1084629 (2022).
26. Meo, A. et al. Magnetization dynamics of granular heat-assisted magnetic recording media by means of a multiscale model. *Phys. Rev. B* **102**, 174419. https://doi.org/10.1103/PhysRevB.102.174419 (2020).
27. Pantasri, W., Meo, A., Chantrell, R. W., Chureemart, P. & Chureemart, J. Granular micromagnetic HAMR model: Investigation of damping dependence and parametric optimization for high performance. *J. Phys. D Appl. Phys.* **57**, 085001. https://doi.org/10.1088/1361-6463/ad0f5d (2023).
28. Jiao, Y., Liu, Z. & Victora, R. H. Renormalized anisotropic exchange for representing heat assisted magnetic recording media. *J. Appl. Phys.* **117**, 17E317. https://doi.org/10.1063/1.4916184 (2015).
29. Natekar, N. A., Hsu, W.-H. & Victora, R. H. Calculated dependence of FePt damping on external field magnitude and direction. *AIP Adv.* **7**, 056004. https://doi.org/10.1063/1.4973800 (2017).
30. Ghoreyshi, A., Saunders, D. A. & Rea, C. J. Thermal erasure in heat-assisted magnetic recording. *IEEE Trans. Magn.* **57**, 1–5. https://doi.org/10.1109/TMAG.2020.3044225 (2020).
31. Hohlfeld, J., Zheng, X. & Benakli, M. Measuring temperature and field profiles in heat assisted magnetic recording. *J. Appl. Phys.* **118**, 064501. https://doi.org/10.1063/1.4928310 (2015).
32. Saunders, D. A., Zhou, H., Rea, C. & Czoschke, P. Magnetic field strength measurements in heat-assisted magnetic recording. *IEEE Trans. Magn.* **55**, 1–5. https://doi.org/10.1109/tmag.2019.2936205 (2019).
33. Hovorka, O. et al. The curie temperature distribution of FePt granular magnetic recording media. *Appl. Phys. Lett.* **101**, 052406. https://doi.org/10.1063/1.4740075 (2012).
34. Meo, A. et al. Signal-to-noise ratio in heat-assisted-recording media: A comparison between simulations and experiments. *Phys. Rev. Appl.* **19**, 054010. https://doi.org/10.1103/PhysRevApplied.19.054010 (2023).
35. Evans, R. F. L. et al. Stochastic form of the Landau-Lifshitz-Bloch equation. *Phys. Rev. B* **85**, 014433. https://doi.org/10.1103/PhysRevB.85.014433 (2012).
36. Chubykalo-Fesenko, O., Nowak, U., Chantrell, R. W. & Garanin, D. Dynamic approach for micromagnetics close to the curie temperature. *Phys. Rev. B* **74**, 094436. https://doi.org/10.1103/PhysRevB.74.094436 (2006).
37. Beaurepaire, E., Merle, J.-C., Daunois, A. & Bigot, J.-Y. Ultrafast spin dynamics in ferromagnetic nickel. *Phys. Rev. Lett.* **76**, 4250–4253. https://doi.org/10.1103/PhysRevLett.76.4250 (1996).
38. Kazantseva, N., Nowak, U., Chantrell, R. W., Hohlfeld, J. & Rebei, A. Slow recovery of the magnetisation after a sub-picosecond heat pulse. *Europhys. Lett.* **81**, 27004. https://doi.org/10.1209/0295-5075/81/27004 (2008).
39. Computer code vampire 5, vampire.york.ac.uk.
40. Evans, R. F. L. et al. Atomistic spin model simulations of magnetic nanomaterials. *J. Phys. Condens. Matter* **26**, 103202. https://doi.org/10.1088/0953-8984/26/10/103202 (2014).
41. Ellis, M. O. A., Ababei, R.-V., Wood, R., Evans, R. F. L. & Chantrell, R. W. Manifestation of higher-order inter-granular exchange in magnetic recording media. *Appl. Phys. Lett.* **111**, 082405. https://doi.org/10.1063/1.4990604 (2017).
42. Garanin, D. A. Fokker-Planck and Landau-Lifshitz-Bloch equations for classical ferromagnets. *Phys. Rev. B* **55**, 3050–3057. https://doi.org/10.1103/PhysRevB.55.3050 (1997).
43. Asselin, P. et al. Constrained Monte Carlo method and calculation of the temperature dependence of magnetic anisotropy. *Phys. Rev. B* **82**, 054415. https://doi.org/10.1103/PhysRevB.82.054415 (2010).
44. Strungaru, M., Ruta, S., Evans, R. F. & Chantrell, R. W. Model of magnetic damping and anisotropy at elevated temperatures: Application to granular FePt films. *Phys. Rev. Appl.* **14**, 014077. https://doi.org/10.1103/PhysRevApplied.14.014077 (2020).
45. Meo, A., Chureemart, P., Chantrell, R. W. & Chureemart, J. The role of interfacial intermixing on HAMR dynamics in bilayer media. *J. Phys. Condens. Matter* **34**, 465801. https://doi.org/10.1088/1361-648X/ac916d (2022).
46. Mryasov, O. N., Nowak, U., Guslienko, K. Y. & Chantrell, R. W. Temperature-dependent magnetic properties of FePt: Effective spin Hamiltonian model. *Europhys. Lett.* **69**, 805–811. https://doi.org/10.1209/epl/i2004-10404-2 (2005).
47. Kazantseva, N., Hohlfeld, J., Rebei, A., Chantrell, R. W. & Nowak, U. Dynamic response of the magnetization to rapid heating in the picosecond regime. *2006 IEEE International Magnetics Conference (INTERMAG)* 41–41. https://doi.org/10.1109/INTMAG.2006.375541 (2006).
48. Ellis, M. O. & Chantrell, R. W. Switching times of nanoscale FePt: Finite size effects on the linear reversal mechanism. *Appl. Phys. Lett.* **106**, 1–5. https://doi.org/10.1063/1.4919051 (2015).
49. Hernandez, S. et al. Geometrical scaling limits of heat-assisted magnetic recording. *IEEE Trans. Magn.* **57**, 1–5. https://doi.org/10.1109/TMAG.2020.3040497 (2021).

Acknowledgements

J. C. and P. C. would like to acknowledge the financially support from Mahasarakham University. R. W. C. gratefully acknowledge the support from Mahasarakham University Development Fund. W. P. would like to acknowledge PhD funding from Seagate technology (Thailand).

Author contributions

J.C., P.C., R.W.C., and A. Suntives conceived and designed the WCAP analysis study. W.P. and A.M. developed the code. W.P. and A.M. performed the simulations. K. Pituso provided the experimental data. All authors analyzed the data and contributed to writing the manuscript.

Additional information

Correspondence and requests for materials should be addressed to J.C.

Reprints and permissions information is available at www.nature.com/reprints.

Publisher's note Springer Nature remains neutral with regard to jurisdictional claims in published maps and institutional affiliations.

Open Access This article is licensed under a Creative Commons Attribution-NonCommercial-NoDerivatives 4.0 International License, which permits any non-commercial use, sharing, distribution and reproduction in any medium or format, as long as you give appropriate credit to the original author(s) and the source, provide a link to the Creative Commons licence, and indicate if you modified the licensed material. You do not have permission under this licence to share adapted material derived from this article or parts of it. The images or other third party material in this article are included in the article's Creative Commons licence, unless indicated otherwise in a credit line to the material. If material is not included in the article's Creative Commons licence and your intended use is not permitted by statutory regulation or exceeds the permitted use, you will need to obtain permission directly from the copyright holder. To view a copy of this licence, visit http://creativecommons.org/licenses/by-nc-nd/4.0/.

© The Author(s) 2025